NUMERICAL COMPUTATIONS OF STORM SURGES WITH BOTTOM STRESS

CHESTER P. JELESNIANSKI

Institute for Oceanography, ESSA, Silver Spring, Md.

ABSTRACT

A linear form of the transport equations of motion is used to compute numerically storm surges generated by model tropical storms traveling across model basins. The storms move in any fixed direction and speed relative to a straight line coast and have a restricted number of physical parameters to fix their strength and size. These parameters are readily available in most weather stations.

A dissipating mechanism, introduced by Platzman, using only an eddy viscosity coefficient is modified to include a bottom slip current by means of a bottom slip coefficient. These two coefficients are used to control the amplitude of resurgences on the sea following the passage of tropical storms. Numerical values for the coefficients are empirically determined by comparing computed and observed resurgences off Atlantic City.

Nomograms prepared from the computations may have some skill in forecasting future storm surges.

1. INTRODUCTION

The storm surge prediction problem is concerned with the rise of coastal waters brought about by meteorological storms. The rising waters not only inundate coastal areas but also act as a pathway for short surface or wind waves to move and break farther inland. It is the purpose of this paper to provide some further insight into the mechanics and prediction of storm surges.

The response of the sea, from driving forces generated by a moving tropical storm, is of such complexity that practical results are obtained only through bold assumptions and empirical tests using numerical computations; an electronic computer, therefore, is viewed as a laboratory to compute storm surges using model storms traveling across model basins. The entire response of the sea, however, is much too general for storm surge computations and only portions of the response are considered.

In the natural oceans there is a basic flow composed of the general circulation, varying seasonally, and the daily astronomical tide. The present state of knowledge and data acquisition for hurricane conditions on the open coast does not permit a direct incorporation of the basic flow into the storm surge computations, nor provide the ability to consider nonlinear interactions with storms. For this reason, and as a great mathematic convenience, only linearized forms of the equations of motion are used in the present study.

The basic flow can be partially accounted for in the computations by appending the predicted astronomical tide and the observed, extrapolated, or predicted seasonal variations of the sea surface to the computed storm surge via the superposition principle (Harris [3]). This is feasible if the effects of nonlinear interactions are small; in any case these corrections can be applied only at shore stations where data are available and not in the open sea.

Model tropical storms have been used by Jelesnianski [6] to compute storm surges but without considering bottom stress in the storm surge equations of motion. The computed surges were found to be reasonable for fast moving storms making landfall but had serious deficiencies for storms moving slowly or traveling parallel to the coast at any speed. Computations therefore were restricted to storms traveling at moderate or higher speeds and with direction of travel at not too acute a crossing angle to the coast. For convenience, storms moving from land to sea were omitted even though the computed surges were reasonable.

A detailed description is given in this paper to surges generated by storm travel inadmissible in the previous paper [6]. These particular surges are complicated in space and time. The techniques developed in [6] to predict storm surges using a restricted number of meteorological parameters are extended to consider storms crossing the coast at any angle and speed, as well as storms traveling parallel to the coast at any speed and distance from the coast. To consider this broad spectrum of storm velocity relative to a coast, methods of applying bottom stress in the numerical computations are necessary. The methods used are useful palliatives in the absence of a sound theory for bottom stress and dissipating mechanisms.

The addition of a bottom stress in the equations of motion does not significantly change the results of [6] but does have a commanding effect with storm travel inadmissible in [6]. Storms traveling parallel to the coast at any speed, or landfalling at slow speeds, form second order surge oscillations due to initialization effects and special wave phenomena, all of significant amplitude; these are superimposed on the generated surge and can be controlled by a dissipating mechanism.

Test computations show that certain portions of the coastal surge profile are almost unaffected when using any

bottom friction law, including a no-friction law if the storm is not moving too slowly. For an observer on sea, facing land, and watching a storm landfalling, the coastal profile and peak surge to the right of landfall are not greatly affected; on the other hand, the profile to the left of landfall is sensitive to the type of bottom stress law used.

2. EQUATIONS OF MOTION FOR STORM SURGE COMPUTATIONS

The model in this study corresponds to that of the previous report [6], except for the addition of bottom stress, and consists of an analytically described storm traveling across a rectangular shaped, variable depth basin that is open to the sea on three sides. Initially the sea in the basin is assumed at rest, and the storm is allowed to grow to maturity from zero strength in a rapid but continuous manner.

In storm surge computations, we are primarily interested in the height of the sea surface and only casually in the current field. It is convenient then to transform the equations of motion to two-dimensional transport fields. This transformation, however, presents serious problems with bottom stress.

For future use we shall need a continuity transport equation which can be written as (Welander [20]):

$$\frac{\partial h}{\partial t}=-\left[\frac{\partial U}{\partial x}+\frac{\partial V}{\partial y}\right] \tag{1}$$

where

$(U, V)=\int_{-D}^{h}(u, v)dz'$, i.e., transport components

h=storm surge (height of mean sea surface above equilibrium level)

u, v=horizontal components of current field

D=depth of the sea

x, y, z'=right hand coordinate system (z' in anticipation of scaling).

The momentum equations of motion (not yet in transport form) with hydrostatic approximation can be written in linear and complex form (Welander [20]) as:

$$\frac{\partial w}{\partial t}=q-ifw+\frac{\partial}{\partial z'}\left(\nu\frac{\partial w}{\partial z'}\right) \tag{2}$$

where

$$w=u+iv,\quad q=-g\left[\frac{\partial(h-h_0)}{\partial x}+i\,\frac{\partial(h-h_0)}{\partial y}\right]$$

ν=vertical kinematic eddy viscosity

f=Coriolis parameter (constant)

g=gravity

h_0=inverse barometer effect (hydrostatic height due to surface pressure).

The last equation considers inertio-gravitational waves since the Coriolis parameter is not varied. This was purposely done for the storm surge is small compared to the scale length of planetary waves. For similar reasons a map scale factor is not considered. Lateral stresses are excluded since the vertical stress influenced by the surface wind is believed to be much larger over most of the area of interest.

To formulate transport fields, one may directly integrate (2) in the vertical to obtain

$$\frac{\partial W}{\partial t}=Q-ifW+\tau_s-\tau_b \tag{3}$$

where

$$\tau_s,\ \tau_b=\nu\frac{\partial w}{\partial z'}\Big|_{z'=0,\ -D}\quad\text{complex form of surface, bottom stress} \tag{4}$$

W=complex form for transports

$Q=Dq$.

The surface stress can be formulated as a function of the wind, but the bottom stress depends on the vertical gradient of the bottom current. Since only transport terms are available if (3) is used directly, it has been customary to assume the bottom stress as a simple quadratic function of transport in conformity with experiments from pipe or channel flow; corrections to such an empirical law for a system under the influence of a surface wind stress has been given by Reid [16]. This type of bottom stress will not be considered since computational experiments gave results that were not always satisfactory.

Other systems of representing bottom stress, which are linear in nature, have been designed by Nomitsu [9], [10], [11], [12]; Nomitsu and Takegami [13], [14]; and Platzman [15]. Platzman's scheme is more convenient for numerical computations. In what follows, we will adhere to the notation given by Platzman whenever possible.

Let the surface boundary condition be $\nu(\partial w/\partial z')|_{z'=0}=R$, where R is the complex form of the surface wind stress, taken as

$$R=\frac{C\rho_a}{\rho}|V_s|V_s$$

where V_s=complex wind, ρ_a, ρ=air, water density, C is assumed to be a constant drag coefficient, and $C\rho_a/\rho=3\times10^{-6}$. We formulate the bottom boundary condition as

$$\nu\frac{\partial w}{\partial z'}\Big|_{z'=-D}=sw|_{z'=-D} \tag{5}$$

where s is a slip coefficient; here we are assuming a "gliding" current above a very thin boundary or skin layer, where for practical purposes the depth of the skin layer is taken as zero.

If only one friction parameter consisting of an eddy viscosity coefficient is used, then computations show that the storm surge is somewhat sensitive to small changes of the parameter. The introduction of a slip coefficient as a second friction parameter greatly reduces this sensitivity

and also gives more freedom when working with dependent data to better fit computed and observed surge profiles.

It is convenient to make the vertical coordinate non-dimensional by the transformation $z=z'/D$. If the time derivative in (2) is treated as an operator, and the resulting second order differential equation with variable z is solved with surface and bottom boundary conditions, then

$$wD=\frac{\sinh \sigma z}{\eta_\nu \nu} R+\frac{\cosh \sigma z}{\eta_\nu \sigma \sinh \sigma}(\cosh \sigma R-sw_{-1})+\frac{1}{\eta_\nu \sigma^2} Q \quad (6)$$

where

$$\eta_\nu=\nu/D^2$$

$$\sigma^2=\eta_\nu^{-1}\left(if+\frac{\partial}{\partial t}\right)$$

$$w_{-1}=\frac{\sigma R+(\sinh \sigma) Q}{D\left[\eta_\nu \sinh \sigma+\frac{s}{D}\sigma \cosh \sigma\right]}=\text{complex bottom current.}$$

If (6) is now integrated in the vertical (with respect to z from -1 to 0), the result is

$$\eta_\nu[\sigma^2+G(\sigma)]M=Q+[1+H(\sigma)]R \quad (7)$$

where

M=complex transport
(equivalent to dimensionalized W in (3))

$$G(\sigma)=\frac{\sigma^2}{\left[\left\{\frac{\nu\sigma^2}{sD}\right\}+\sigma \coth \sigma-1\right]}$$

$$H(\sigma)=\frac{1-\frac{\sigma}{\sinh \sigma}}{\left[\left\{\frac{\nu\sigma^2}{sD}\right\}+\sigma \coth-1\right]}.$$

For the purposes of integration with respect to z, and of algebraic manipulation, the operators, σ, $G(\sigma)$, σ^2, $H(\sigma)$, etc., can be treated as ordinary algebraic quantities and parameters, save that the operator must remain to the left of some operand, such as M, Q, or R in equation (7).

The meaning of a compound operator such as $G(\sigma)$, $H(\sigma)$, etc. is based on power series expansions in σ; e.g.,

$$\sigma(\sinh \sigma)F(t)=[\sigma^2+\frac{\sigma^4}{3!}+\frac{\sigma^6}{4!}+\ldots]F(t)$$

(where the terms of the power series are just the same as those of a function $z \sinh z$) provided the series converges. When it does not converge directly, means similar to analytic continuation can be employed to get the result of the operator; these means lead to a unique result.

Equation (7) was formed to set Q by itself; it is just as easy to set $\sigma^2 M$ by itself if this is desired. The choice of which term is set by itself can be governed by the nature of the numerical scheme to be used.

Note that for $s=0$, G and H are zero; (7) is then no more than (3) *without* bottom stress, i.e., frictionless flow. Platzman [15] treated exclusively the special case, $s=\infty$, or $w_{-1}=0$, i.e., no bottom slip. This is equivalent to assuming that the horizontal velocity gradually approaches zero near the bottom. However, the horizontal velocity near the bottom is often quite large (excepting a thin boundary layer which is not included in the present analysis). In order to recognize the existence of this boundary layer without being concerned with its detailed structure we have taken bottom stress (5) as proportional to a slip velocity assumed to glide over the top of the bottom boundary layer. Our results with idealized storms appear to point out that ν controls the peak surge on the coast, whereas s controls the dispersion of the surge especially to the left of the storm center on the coast.

The difficulty in applying equation (7) lies in representing the operators $G(\sigma)$ and $H(\sigma)$ numerically. The functions M, R, and their first derivatives in time can be readily approximated directly from available information, but higher derivatives resulting from a Taylor's expansion of $G(\sigma)$ and $H(\sigma)$ are more difficult to obtain.

Accordingly, Platzman suggests that G and H be approximated by truncating their Taylor's expansion about $\sigma_0^2=ifD^2/\nu$ to obtain

$$G(\sigma)\simeq G_0(\sigma_0)+\frac{D^2}{\nu} G_1(\sigma_0)\frac{\partial}{\partial t};\ H(\sigma)\simeq H_0(\sigma_0)+\frac{D^2}{\nu} H_1(\sigma_0)\frac{\partial}{\partial t} \quad (8)$$

where the subscripts represent the zeroth and first derivatives with respect to σ^2, and the derivatives are evaluated at $\sigma^2=\sigma_0^2$. Using the approximation (8), equation (7) takes on the simpler form

$$\frac{\partial M}{\partial t}=BQ-ifAM+\left[C+\frac{J}{if}\frac{\partial}{\partial t}\right]R \quad (9)$$

where

$$A=\frac{1+\sigma_0^2 G_0}{1+G_1},\ B=\frac{1}{1+G_1},\ C=\frac{1+H_0}{1+G_1},\ J=\frac{\sigma_0^2 H_1}{1+G_1}.$$

Numerical tests using (9) gave good results for slow-moving storms, but spurious waves formed, especially along the storm's track, with fast-moving storms. When the J term was dropped the spurious waves did not occur. This situation prompted a closer look at the truncated forms of (8) to see whether they are sufficiently representative for storm surge computations, and whether the J term is important or not. (See Appendix I.)

Equation (9) with the J term omitted has the real and imaginary parts

$$\left.\begin{aligned}\frac{\partial U}{\partial t}&=-gD\left[B_r\frac{\partial(h-h_0)}{\partial x}-B_i\frac{\partial(h-h_0)}{\partial y}\right]\\&\quad+f[A_rV+A_iU]+C_r^{(x)}\tau_s-C_i^{(y)}\tau_s\\\frac{\partial V}{\partial t}&=-gD\left[B_r\frac{\partial(h-h_0)}{\partial y}+B_i\frac{\partial(h-h_0)}{\partial x}\right]\\&\quad-f[A_iU-A_rV]+C_r^{(y)}\tau_s+C_i^{(y)}\tau_s\end{aligned}\right\} \quad (10)$$

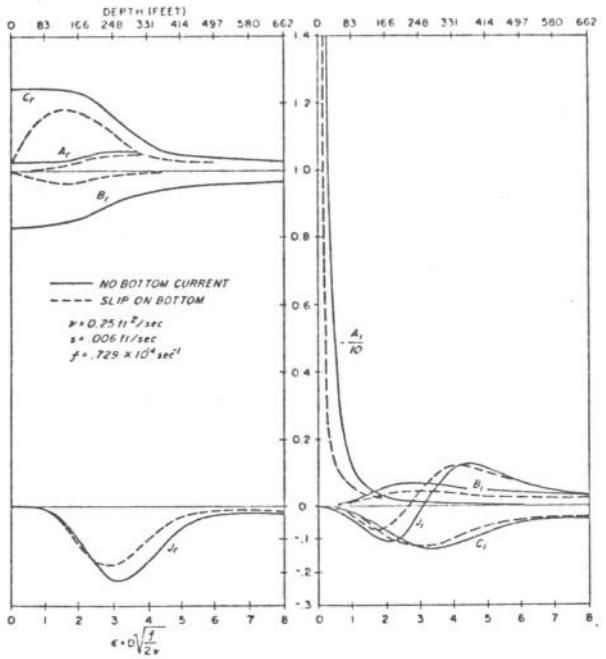

FIGURE 1.—Real and imaginary parts of the four coefficients (A, B, C, J) of equations (9) and (17) as functions of Ekman number "ϵ" or depth.

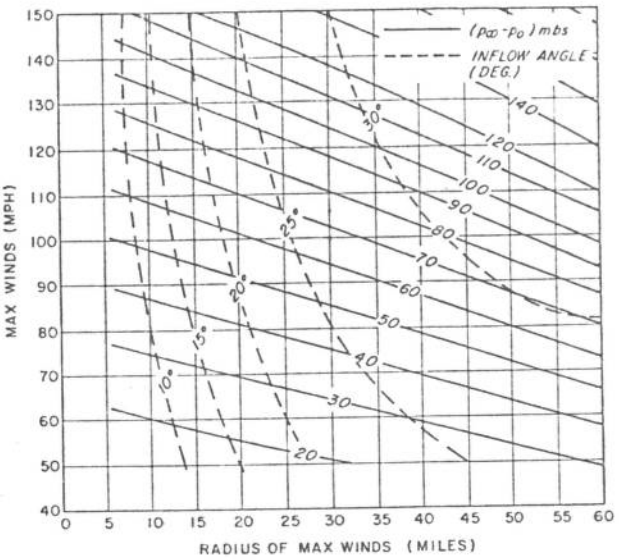

FIGURE 2.—A nomogram relating three model storm parameters, stationary storm maximum wind, radius of maximum wind in statute miles, and pressure drop. The inflow angle occurs 100 mi. from the storm center. The storm center is at latitude 30°.

These equations involve only first derivatives with respect to time. The six subscripted functions (A, B, C) are dependent only on depth when eddy viscosity and bottom slip coefficients are specified; their form is given in figure 1.

The numerical scheme for (10) used in this study is given in Appendix II. An heuristic approach to form values for the eddy viscosity coefficient ν, and slip coefficient s, is given in Appendix III.

In this study, the parameters describing the model storms and basins have a range usually less than an order of magnitude. Thus, in dealing with the drag coefficient of the surface wind stress as well as eddy viscosity and slip coefficients, we have tacitly assumed constant values as sufficiently serviceable for the range of parameters in this report. This means that the results of the computations are restricted mainly to tropical storms.

3. GEOGRAPHICAL ORIENTATION, STORM PARAMETERS, DEPTH PROFILES, DEFINITIONS

For purposes of orientation in the following sections, the observer will always be at sea and facing the coast. The coast to his right will be considered relative north, to his left relative south. Crossing angles of the storm's path to this orientated coast will be described in meteorological sense; thus a storm on the coast moving from relative north has a crossing angle of 0°, moving normal to the coast from sea, a crossing angle of 90°, etc.

There are five simple parameters to describe the strength, size, and motion of a model storm; these in turn determine the driving forces of surge generation, the pressure gradient, and wind stress. The parameters are:

(1) *Latitude.*—Normally the latitude of the storm's landfall; if the storm does not landfall, the latitude of a point of interest on the coast. The storm surge is only mildly sensitive to this parameter and varies by less than 10 percent between latitudes 15° and 45°, all other parameters being the same. For this reason and because we are interested in transient effects as opposed to general circulation, latitude is not varied in the equations of motion.

(2) *Radius of Maximum Winds.*—The distance from the storm center to the maximum wind of the storm. This distance is not dependent on storm motion, and for any given time it is assumed to be the same in all directions. This parameter controls the horizontal extent of the surge on the coast. If only the value of the peak surge on the coast is desired then the accuracy of this parameter becomes unimportant, and for most purposes a rough estimate of this distance is sufficient.

(3) *Pressure Drop of the Storm.*—The pressure difference from the center to the periphery of the storm. For an actual storm, this could be the mean of several differences measured along rays from the storm center to the first anticyclonically turning isobar. This is the most important storm parameter; it controls the peak surge on the coast. For a *fixed* pressure drop, the peak surge on the coast is only weakly dependent on the radius of maximum wind. The pressure drop is not used directly in the model computations, instead it is used as an argument (fig. 2)

to arrive at a more convenient measure for computations, the *stationary-storm-maximum-wind*. In the previous report a simple Newton-Raphson integration method was used to derive the nomogram; in this report the more precise Runge-Kutta method was used. The differences are only minor.

(4) *Speed of Storm.*—Rate of motion of the storm center. With all other parameters held fixed, there is a critical storm speed that gives the highest peak surge on the coast.

(5) *Direction of Storm.*—Direction of motion of the storm center. With all other parameters held fixed, there is a critical direction of storm motion which gives the highest peak surge on the coast.

The computed surge depends on the depth contours of the basin as well as the model storm. The continental shelf of the oceans vary predominantly in one direction, therefore a one-dimensional *depth profile* is used in the model. This profile is used solely for convenience in the present stage of developing the dynamic model. There are no essential difficulties in the use of two-dimensional bottom specifications when such detail is desired or when its effect is believed to be significant relative to other terms.

For further reference it is convenient to make the following definitions:

Standard Storm.—A model storm having a *stationary-storm-maximum-wind* of 100 m.p.h. and with storm center at latitude 30°.

Standard Basin.—A model basin having a *linear* sloping depth profile consisting of a 3-ft. drop for each mile length along the continental shelf, a 15-ft. depth at the coastal boundary, a shelf length of 60 mi., and a deep water open boundary depth of 195 ft. This basin has a slightly larger slope near the coast than the standard basin of the previous report [6]; hence computed surges from a standard storm in this basin are slightly smaller than those in the previously used basin. In the numerical model, for a given depth profile, the storm surge is only weakly dependent on any alteration of the immediate slope at the coast of the continental shelf; therefore a vertical wall is substituted at the coast with finite depths at the coastal boundary.

Coastal Surge Profile.—A plot or snapshot picture of the surge heights along the coastline for a given time.

Directly Generated Surge.—Storms traveling parallel to the coast can generate traveling and/or standing waves superimposed on the coastal surge profile. The first crest and trough of the coastal surge profile associated with the storm's center, and moving with the storm, is the *directly generated surge*. Figure 3 illustrates the motivation for this definition; notice that fast moving storms traveling parallel to the coast can generate traveling waves behind the storm's track and these traveling waves amplify that portion of the directly generated surge behind the storm's track, i.e., storms moving to the right amplify the directly generated trough, storms moving to the left amplify the directly generated crest.

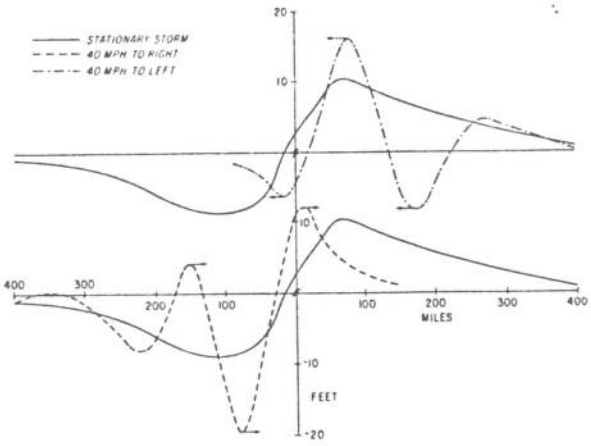

FIGURE 3.—Plots of computed coastal surge profiles generated by a storm moving to the right, and moving to the left along the coast; and then compared to a stationary storm, center of storm remains on coast.

Resurgences.—At any point on the coast, large amplitude oscillations of the surge can occur with time for storms moving parallel to the coast. These oscillations, excluding passage of the *directly generated surge*, will be called *resurgences*. The resurgences can be shelf seiches or edge waves (Munk et al. [8], Reid [17]). Shelf seiches also occur for slowly moving storms making landfall; this is a special type of resurgence, generally with higher harmonics and usually of small amplitude unless the storm is moving very slowly.

4. GROWTH TIME OF STORM, INITIALIZATION, AND SPECIAL WAVE PHENOMENA

The growth time to maturity for fast moving storms making landfall, and traveling at not too small a crossing angle to the coast, was found empirically to be of trivial concern. For storms traveling parallel or nearly parallel to the coast at any speed, initialization phenomena dependent on growth time and of significant amplitude are generated or superimposed on the surge profile.

In order that the peak surge have only weak dependence on initial storm placement, it was necessary initially to place landfalling storms at least past the continental shelf (the deep water open boundary) or to place storms traveling from land to sea at the mirror image point; storms traveling parallel or at a small angle to the coast required an initial placement based on several criteria that will now be discussed.

Figure 4 shows the *directly generated crest* plotted against time in the case of a *stationary*, standard storm with center on the coast of a standard basin. This peak surge with time acts similarly to a damped-forced oscillator. The transient oscillations result from rapid growth to maturity of the storm; they cannot be completely eliminated for any

reasonable growth time in the computations. Over a wide range of growth time the phase varied but the amplitude of the second crest of the transient oscillations was nearly constant. Henceforth, we shall always use 100 min. as a growth time solely for convenience. We adopt a working criterion that whenever transient oscillations of this nature occur, the second crest will be chosen as representative of the peak surge on the coast; the same type of transient oscillations will affect the moving directly generated surge. Thus for a working criterion, the initial placement of the storm center in the model basin must be sufficiently distant from the point of interest so that a second crest has time to form.

Figure 4 also shows the surge with time for the point on the coast having peak surge in the case of a stationary storm placed 80 mi. from the coast. Here, there is a continuous growth of the surge with time, i.e., it takes time for the surge to build on the coast; notice that higher harmonic oscillations occur for this case. Henceforth, for a working criterion, we shall adopt the computed peak surge 8 hr. after initialization as a representative value for those cases where the coastal surge displays many variations with time.

The damped-transient oscillations, superimposed on the directly generated surge from initialization processes, is not the only phenomenon occurring with storms traveling parallel to the coast. There are also the phenomena of standing waves, traveling waves, or a combination of both superimposed on the surge profile behind the storm's track; there are even further complications if the storm is varying in strength, size, and speed with time.

As an example of these complexities, consider the September 1944 storm which moved parallel to the Eastern Seaboard (this storm is discussed in Appendix III; its track is given in figure 20 and the generated surge at Atlantic City in figure 21). Figure 5 pictures the entire computed coastal surge profile against time. Notice that the traveling *directly generated* surge associated with the storm center has initially a large transient oscillation that dies out with time, and the directly generated surge becomes smaller with time due to decreasing storm strength with time. In this figure, the oscillations or resurgences with time at Atlantic City, after passage of the directly generated surge, are readily seen to be shelf seiches and not traveling edge waves. The computed resurgences may have been affected by reflective properties inherent in the open boundary conditions of the model; possibly the use of open boundaries with radiative properties would be more appropriate. The two lateral (relative north, south) open boundaries, with normal transport gradient set to zero, do not strongly affect the first few resurgences; this was determined by varying the length of the basin and repositioning the two lateral boundaries on the natural coast. No equivalent tests were made for the deep water open boundary.

In the numerical model, traveling edge waves will predominate over shelf seiches for storms that are *fast* moving,

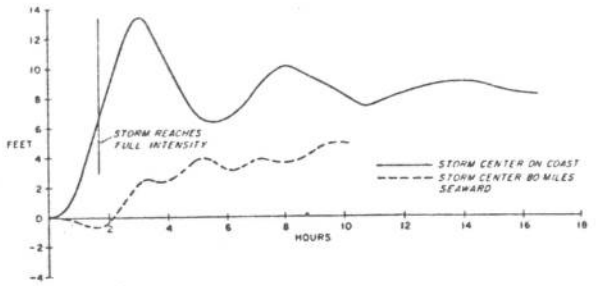

FIGURE 4.—The computed height of the peak surge against time generated by a stationary storm.

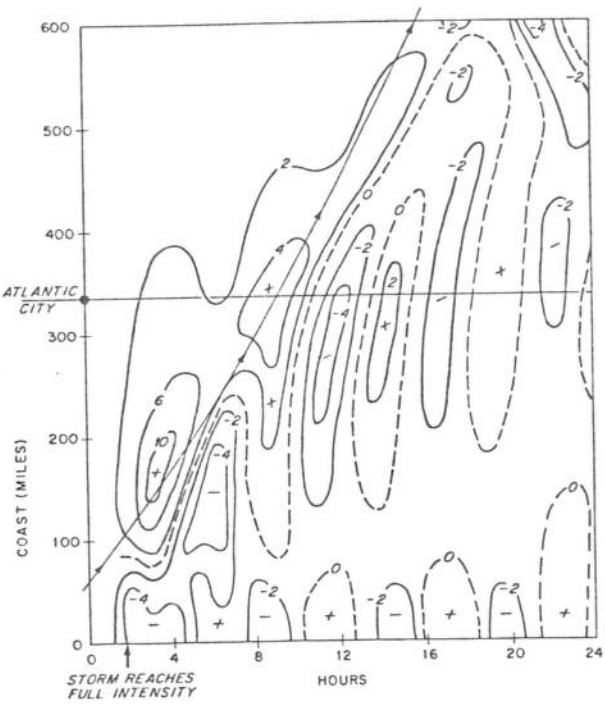

FIGURE 5.—The computed coastal surge profile, contoured against time, for the September 1944 storm modeled in Appendix II. The line with arrows represents the position of the storm center normal to the coast (center of storm 40 mi. seaward). This figure shows the formation of shelf seiches behind the storm's center.

of constant strength, size, and speed, and for basins which have shallower coastal depths and gentler slopes. Consider now the above storm but with constant parametric storm values equivalent to those observed off Atlantic City; consider also a standard basin whose profile differs significantly from that off Atlantic City (fig. 17). Figure 6 pictures the computed coastal surge profile for this hypothetical storm and basin. Notice that the resurgences which form with time behind the storm's track are now traveling waves in contrast to those in figure 5. The

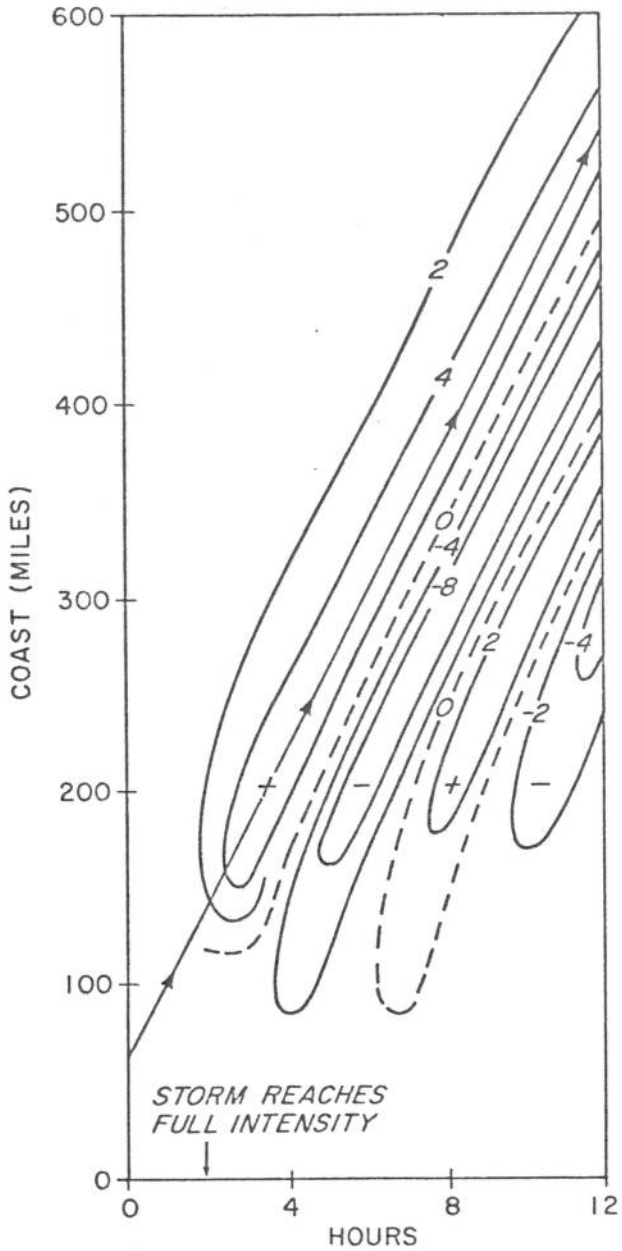

FIGURE 6.—Same as figure 5 for a standard storm, in a standard basin, and traveling parallel to the coast at 40 m.p.h. with center of the storm 40 mi. seaward. This figure shows formation of traveling edge waves on the coast.

directly generated crest does not change in value, except for rapidly decaying initialization phenomena at the beginning of the computations, the directly generated trough is amplified by the traveling edge waves forming behind the storm's track.

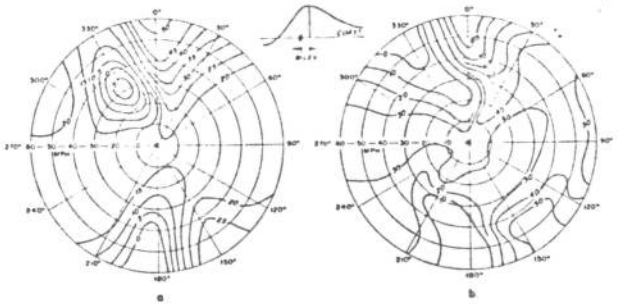

FIGURE 7.—Contours of distance, in statute miles, from landfall position to point of peak surge on the coast. Radii are storm speeds, rays are crossing angles of storm track to the coast (standard storm in standard basin). (a) Radius of maximum wind, 15 statute mi. (b) Radius of maximum wind, 30 statute mi.

For a working convenience, we shall henceforth consider only storms of constant strength and size after reaching maturity, and traveling with uniform rectilinear velocity.

5. LANDFALLING STORMS

Landfalling storms affect only a segment of the coast near the point of landfall; consequently, we are interested not only in the peak surges but also in the horizontal extent or *dispersion* of the surge along the coast. The dispersion is strongly dependent on the radius of maximum winds. These storms, with speed and crossing angle to the coast not too small, do not generate initialization phenomena and resurgences on the surge profile; therefore the generated surge is much less complicated than the examples of the previous section. The peak surge occurs at only one point on the coast, it is generally larger with storms traveling from sea to land.

As a preliminary aid to determine the surge dispersion along the coast, we construct a pre-computed surge profile generated by a *standard* storm, with fixed radius of maximum winds, moving at fixed velocity across a *standard* basin. In what follows, we assume that the position of landfall is known and use it as an origin. To construct this preliminary profile, we use nomograms (figs. 7–15) which give contours of pre-computed distances and heights at selected points along the surge profile. These figures, in polar coordinates, have rays as crossing angles of the storm to the coast, and radii as storm speed. Figures marked (a) and (b) are for storms having 15- and 30-mi. *radius of maximum winds* respectively; presumably one can interpolate for other values of the radius. These diagrams consider variation of three storm parameters; in a later section we shall consider corrections to the pre-computed profile using parameters for any particular storm and basin.

In figures 8 and 9, we have outlined a region in broken lines to call attention to edge wave phenomena which can affect the directly generated crest and trough respectively. An example of this situation is given in figure 3.

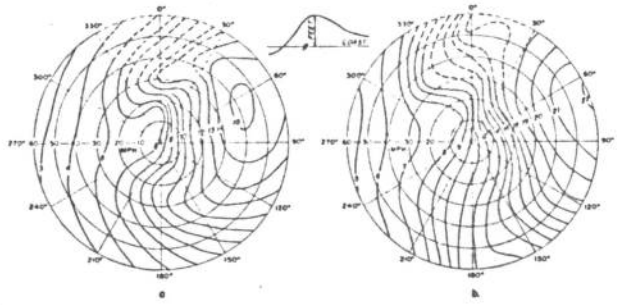

FIGURE 8.—Contours of peak coastal surge values, in feet. Arguments are identical to figure 7. The upper region bounded by broken lines point out edge wave phenomena that could be affecting the directly generated crests in the model computations.

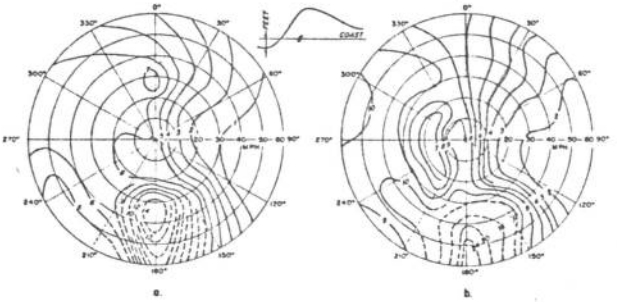

FIGURE 9.—Same as figure 8 for the minimum surge, portrayed at time of the peak surge. The absolute minimum surge does not necessarily occur at time of peak surge.

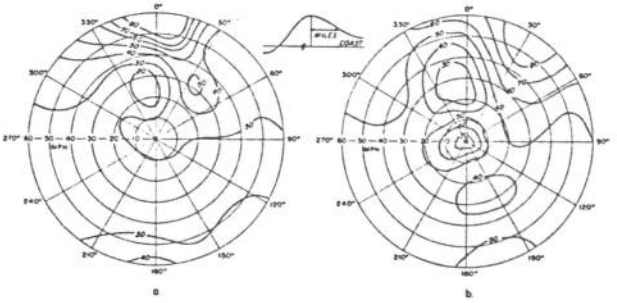

FIGURE 10.—Contours of distance on coast, in statute miles, from point of peak surge to point on coast having ½ the peak surge, to the right of landfall. Arguments same as figure 7.

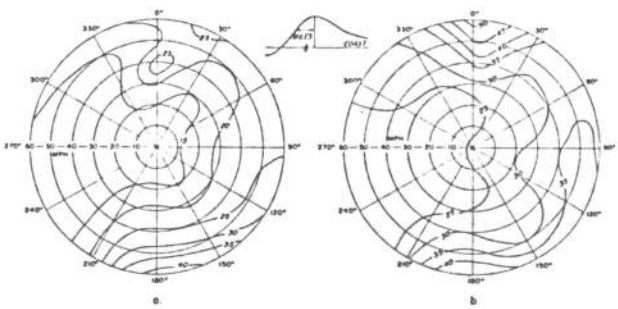

FIGURE 11.—Same as figure 10, but to left of landfall.

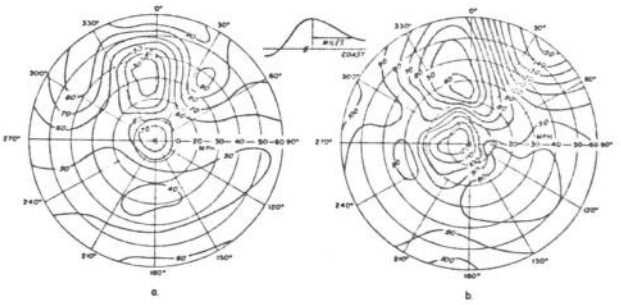

FIGURE 12.—Same as figure 10, but for ¼ peak surge value.

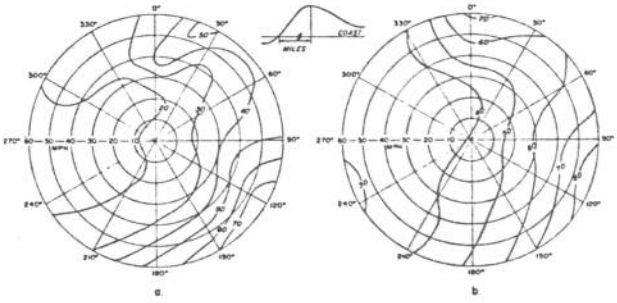

FIGURE 13.—Distance, in statute miles, from peak surge to zero surge on the coast. Arguments same as figure 7.

Very slowly moving and landfalling storms form shelf seiches with phase angle depending on initial storm placement. These seiches are superimposed on the surge; thus, for different storm speeds, there is no *a priori* way to relate phase angle of seiches to peak surge on the coast. Therefore, it was necessary to force continuity of the various contours about the origin of the polar graphs, subjectively; the stationary storm at the origin, with *representative* value, was used as an anchor or invariant. The surges thus derived never differed by more than one-half foot from actual computations. Similar circumstances occurred for storms crossing the coast at a small angle and at any speed.

We emphasize that the constructed profile is only for the time of peak surge on the coast. The absolute minimum surge does not necessarily occur at time of peak surge; the negative surges on the profile are only transitory and eventually can turn to respectable positive values

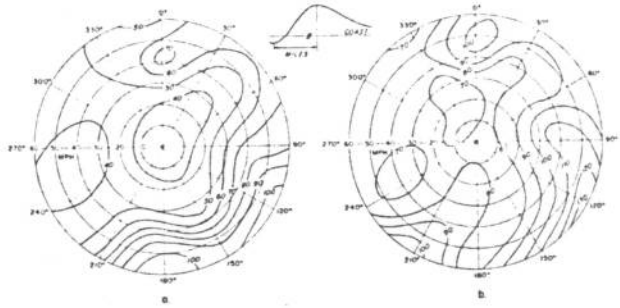

FIGURE 14.—Distance, in statute miles, from peak surge to minimum surge on the coast. Arguments same as figure 7.

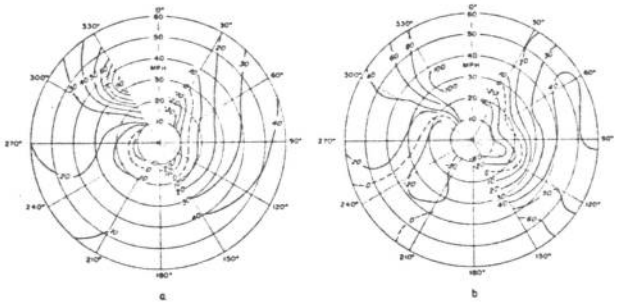

FIGURE 15.—Arrival time, in minutes, of peak surge on the coast after storm landfall. Arguments same as figure 7.

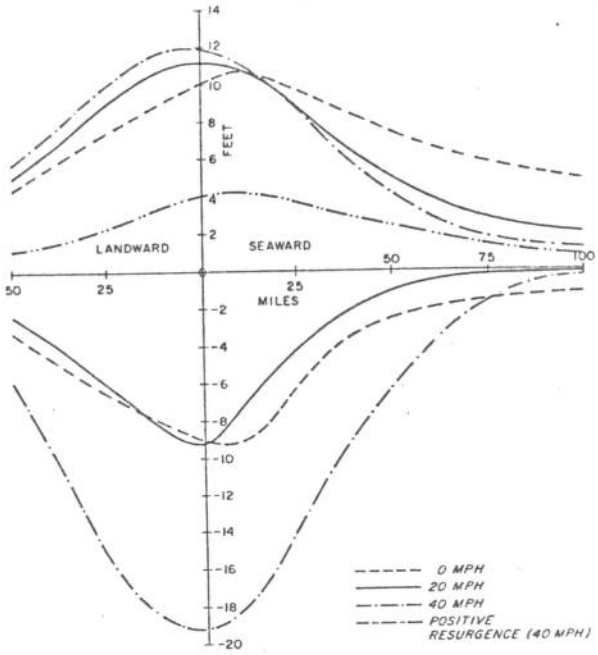

FIGURE 16.—Height nomogram of the directly generated crest and trough, and the resurgence amplitude, for storms (standard storm and standard basin) moving at different speeds parallel to the coast. The abscissa is distance of the storm center from the coast in statute miles.

after passage of the storm. The history of the region of negative surges has not been documented.

The surge profile from a *stationary* storm can be depicted by the nomograms of this section only if the center of the storm rests on the coast. If the storm center is at a distance from the coast, then the heights of the crest and trough can be extracted from figure 16 of the next section and the surge profile completed with the nomograms of this section. We are assuming here that the dispersion of the surge does not depend on distance of the resting storm center from the coast; separate computations show this to be a good assumption.

6. STORMS NOT LANDFALLING

For convenience, we treat all storm motions that stagnate, loop, recurve, or in any way fail to landfall, as storms traveling parallel to the coast. For simplicity, we restrict description of the surges from these storms to the *moving*, directly generated surge and follow the rules set forth in past sections to form representative surge values.

We shall not consider here the form* of the coastal surge profile at fixed times, nor time of passage of crests and troughs on points along the coast.

To construct a nomogram, for purposes of forecasting the directly generated surge from these storms, we consider a standard storm traveling parallel to the coast of a standard basin at particular storm speeds. Let the *radius of maximum winds* be 30 mi.; other values for this storm parameter need not be considered since we are primarily interested in *peak* surge and not seiches and resurgences. We now focus attention on the directly generated crest and trough and note that these are traveling with the storm center along the coast. Figure 16 is a resulting nomogram from a series of computations which give representative values of the directly generated crests and troughs for the storm traveling along the right** side of the coast at various distances from the coast; above the abscissa (miles), positive peak surges are shown, below negative peaks. At large distances from the coast, slowly moving storms have higher surges (the criteria of the previous sections give the surge 8 hr. after initialization; hence there is time for the surge to build), but near the coast fast moving storms have higher surges.

The standard basin of this study favors traveling (edge) waves as opposed to seiches for fast moving storms moving parallel to the coast. One should therefore be careful in accepting these resurgences, and the directly generated

*Stationary storms could be treated as an exception here since the crest and trough remain stationary on the coast. In this case one could be interested in the dispersion on the coast of the stationary surge profile.

**We do not consider travel along the *left* side since this is a rare occurrence limited to lower California and to the western Florida coast.

trough, as fully representative since we have not considered storms that vary in strength, size, and speed, nor depths varying in two dimensions, nor curvilinear coasts, nor the effect of various depth profiles on the resurgences. In the present model these resurgences do not become important unless the storm is very fast moving with center slightly seaward of the coast.

Evidence of *resurgences* (edge waves) does not begin until the storm travels in excess of 20 m.p.h., and not until the storm travels about 40 m.p.h. is there significant amplitude. Figure 16 also shows the amplitude of resurgences for storms traveling at 40 m.p.h. and at time 10 hr. after initialization; notice that the maximum resurgence amplitude occurs slightly seaward of the coast, Greenspan [2]. Only the first resurgence behind the storm's track is shown, and this only after passage of the directly generated surge since the following resurgences are dampened.

Corrections to the pre-computed surge of figure 16, for non-standard storms and basins, are given in the next section.

7. CORRECTING THE PRE-COMPUTED SURGE FOR IN-SITU STORMS AND BASINS

In the development of a practical forecasting system for storm surges, it is desirable to modify the preliminary constructed profiles and surges of the preceding sections for particular storms and basins that differ from standard. The corrections would then be for non-standard values of stationary-storm-maximum wind, latitude, and basin depth profile.

Correcting the pre-computed surges for different values of the parameter, maximum wind, is very easy since the computed surge is almost proportional to the square of the maximum wind (as shown in [6]).

For the *same* pressure drop, the peak surge on the coast is not unduly sensitive to the parameter, radius of maximum wind. This can be verified with the nomograms of figures 2 and 8 and the above correction for the maximum wind since the figure is used only to determine peak surges on the coast.

Variations of the latitude parameter alters the computed surge in only a minor way (see [6]). It was decided as an added convenience to incorporate corrections for latitude with corrections for depth profiles.

Figures 17 and 18 give correction factors F_D for special points along the Eastern Seaboard and Gulf States of the United States to correct the precomputed surge for in-situ depth profiles; corrections for latitude have been incorporated. Presumably interpolation can be used between the special points. The factors were obtained from computations using the given depth profiles at the special points and various storm conditions; they are somewhat subjective since they do change with storm conditions, but in most cases only slightly. The correction factors are for the peak surge and would differ for other points on the surge profile, being least reliable for the negative portion of the surge. We assume the factor, a function of the depth profile normal to the coast, can be used for the pre-computed surge profile providing the storms do not differ greatly from standard. The factors are not invarient when comparing with other varied storm parameters, but they change only slightly for the parametric range of storm values used in this study.

The depth contours of a natural basin vary in two-dimensions, but the variation normal to the coast generally is much greater than the variation parallel to the coast. In this study we compute only for variation of depths in one-dimension and assume the depth correction factors, applied selectively at selected points along the surge profile, are good approximations for two-dimensional basins.

The dispersion of the surge on the coast does not change appreciably when varying the parameters maximum wind and depth profile, but does change some when varying the latitude. For convenience it will be assumed here that the dispersion of the surge remains invariant.

There is a unique region along the Florida coast between Miami and Palm Beach where the bottom depths descend from the coast with extreme rapidity. The model discussed here does not cover this case. South of Miami the depths descend with equal vigor; however, there is a shallow shelf along the coast in this region. It was subjectively decided to give this shelf a length of 10 mi. to arrive at some correction factor for the non-standard depth profile; the reliability of the factor in this area is questionable.

To correct the pre-computed surge heights of the previous sections for non-standard storms and basins along the United States coast, the following could be used at selected points on the coast:

$$h_c = h_s (V_R/100)^2 F_D$$

where h_c is the corrected surge height, h_s is the standard pre-computed surge height, V_R is the stationary-storm-maximum wind parameter, and F_D is the depth profile correction factor (figs. 17 and 18).

8. SUMMARY AND CONCLUSIONS

It is possible to compute a reasonable storm surge tide with a numerical model that uses a simple linearized form of the equations of motion. Bottom stress in these equations was not found to be significant in surge generation with fast moving storms making landfall, but a dissipating mechanism was necessary to control large amplitude resurgences and/or initialization phenomena for storms moving parallel to the coast at any speed, as well as slowly moving storms making landfall.

In this paper, a bottom stress formulation was chosen with certain desirable properties in the generation of the coastal surge profile. These properties were most evident for the range of storm velocity not admissible in a previous report [6]. Some of the properties were suppression of large transports at and near the coast,

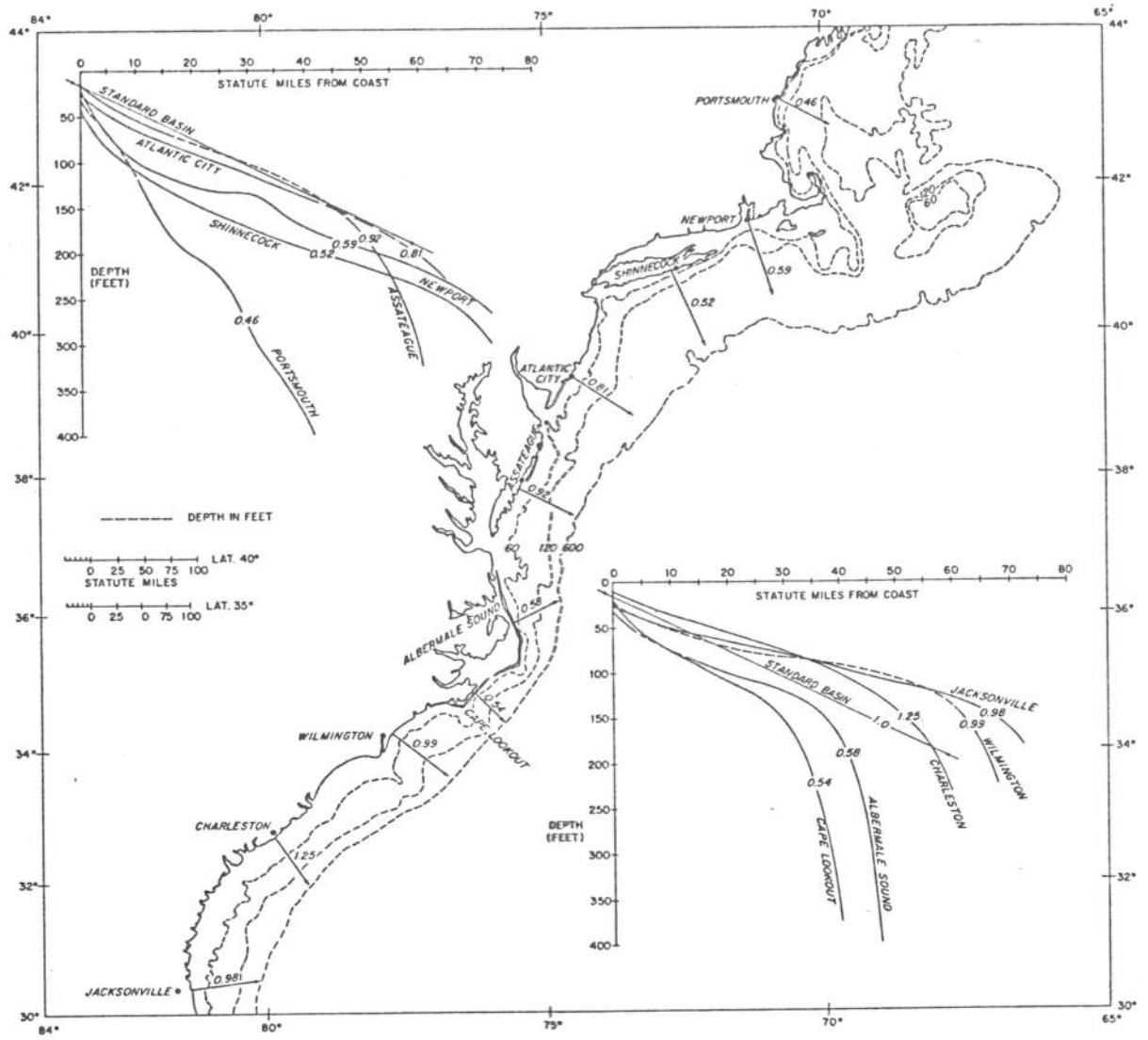

FIGURE 17.—Correction factors at selected points along the Eastern Seaboard of the United States for depth profiles other than standard; the factors are used to correct pre-computed surge heights in a standard basin. The inserts are the *mean* depth profiles of the selected points.

and damping of special wave phenomena and initialization effects generated by storms traveling parallel to the coast. Since non-dimensional analysis shows that the dissipating term is small compared to the inertial term for rapidly moving storms traveling across the continental shelf (Kajiura [7]), values for the friction parameter were chosen so that the coastal surge profile computed with or without bottom stress was nearly identical for fast moving storms traveling at or near normal incidence to the coast. To demonstrate the usefulness of a bottom stress formulation with the above properties, observed surges generated by a fast moving storm at a tide station that was undergoing special wave phenomena and initialization effects were compared with computed surges. To better fit the observed and computed values, the scheme for bottom stress introduced by Platzman [15] was modified to include a bottom slip current.

In [6] a proto-type prediction scheme for forecasting storm surges was introduced. This was done with nomograms that were prepared from pre-computed data using the parameters of a standard storm and a standard basin. In the prediction scheme, a preliminary surge profile

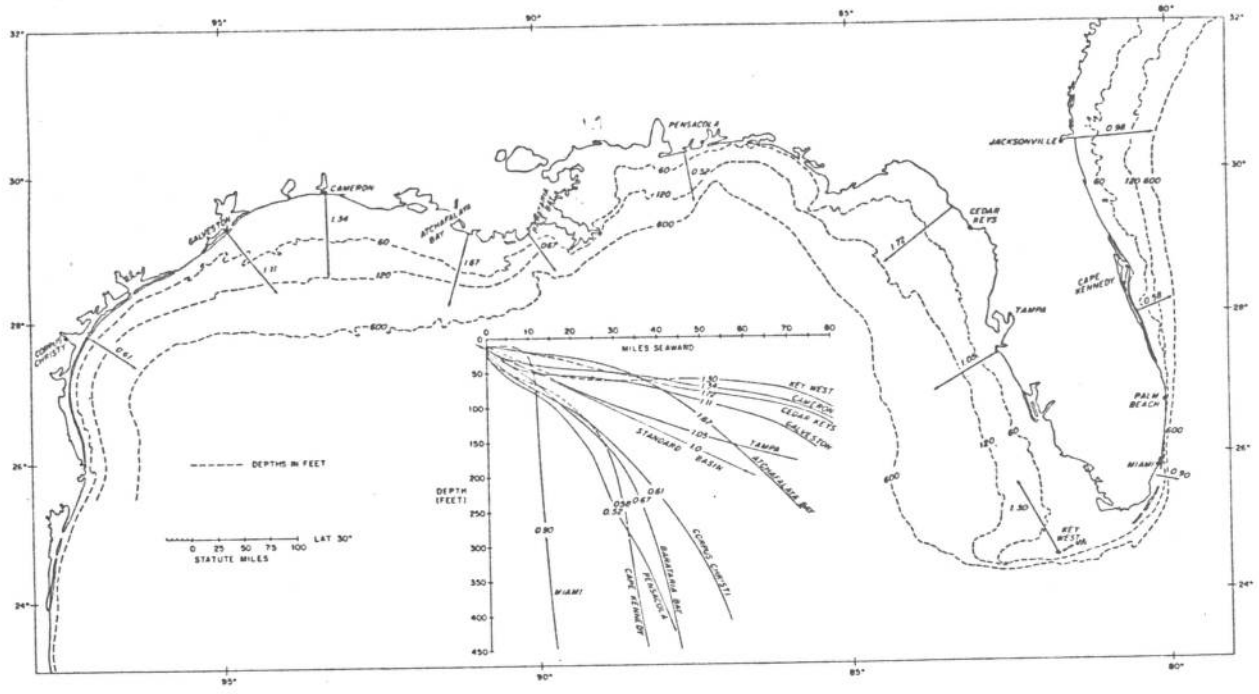

FIGURE 18.—Same as figure 17 for the Gulf States and Florida.

was first constructed from the nomograms; *three* simple correction factors for maximum wind, latitude, and basin depth profile were then used to correct the preliminary profile for in-situ storms and basins that differed from standard. In this report the same scheme is adhered to except that only *two* simple correction factors were used; for simplification, corrections necessary for latitude and basin depth profile were combined as one, at the expense of limiting the predicting scheme to the Eastern and Gulf States of the United States.

Our model does not consider curvilinear boundaries, bays, inlets, etc.; consequently the method of constructing surge profiles from pre-computed nomograms in this study are to be considered only as a preliminary guide for field forecasting purposes.

The important parameters of the storm model are not difficult to ascertain or forecast in weather stations *excepting* the point of landfall. For storms crossing the coast, the distance from landfall to peak surge is roughly equivalent to the radius of maximum winds, and this sets the horizontal scale of the entire surge profile; therefore a high order of accuracy in landfall prediction is required.

The methods of this study consider a straight line coast. Further research is desirable to consider curvilinear boundaries in the model. With this more natural boundary condition it should be possible in the future to prepare in-situ surge forecasts by computer, using forecasted storm parameters and landfall point. The forecasted landfall point would determine the basin to be used as well as the depth contours of the basin.

APPENDIX I

To test the representativeness of equations (8) and (9), we use an heuristic approach (suggested by Dr. A. D. Taylor) that only partially resolves the problem.

Let us consider, for simplicity and illustrative purposes, the case of no bottom slip, i.e., $s=\infty$. Then G and H are

$$G(\sigma)=\frac{\sigma^2\tanh\sigma}{\sigma-\tanh\sigma};\ H(\sigma)=\frac{\tanh\sigma-\sigma\,\mathrm{sech}\,\sigma}{\sigma-\tanh\sigma}. \qquad (11)$$

These operators, regarded as analytic functions of σ, have removable singularity at $\sigma=0$, and simple poles (i.e., zero denominator) on the imaginary axis of σ at approximately $\sigma\simeq\pm i(2n-1)\frac{\pi}{2}$. This implies that if (11) is expanded in power series about a center in the σ plane, not on the imaginary axis, the series will converge in some region about that center.

Suppose one of the operands was the function $Ee^{i(\beta t+\phi)}$ for some complex values E, β, ϕ. Then

$$\frac{\partial}{\partial t}Ee^{i(\beta t+\phi)}=i\beta Ee^{i(\beta t+\phi)}$$

so that the effect of operating with $\partial/\partial t$ is just the effect of multiplying by $i\beta$. An operator formed as a "function" $f(\partial/\partial t)$ has, on the operand $Ee^{i(\beta t+\phi)}$, the effect of multiplying by $f(i\beta)$, for the operand $Ee^{i(\beta t+\phi)}$ the operator $\partial/\partial t$ "takes on the value" $i\beta$.

In general, the operands will not be of the form $Ee^{i(\beta t+\phi)}$; however, at any time t for which the operand is not zero, there is an exponential function which fits most closely to the operand. If the values of E, β, ϕ of the approximating exponential do not rapidly change with time, then it is reasonable to approximate $\partial/\partial t$ with the value $i\beta$.

The values of E, β, ϕ depend on the operands and the time t for which the "evaluation of $\partial/\partial t$" is performed and are different for the operands M and R. If β is real, so that the operand is neither increasing or decreasing in value, the values of G and H will be finite and bounded. Figures 19 a-b give the real and imaginary parts of G and H against σ^2, with $\sigma^2=iD^2(f+\beta)/\nu$ (i.e., replacing $\partial/\partial t$ by $i\beta$). These figures indicate that a linear approximation to G and H may be acceptable, provided β is not large.

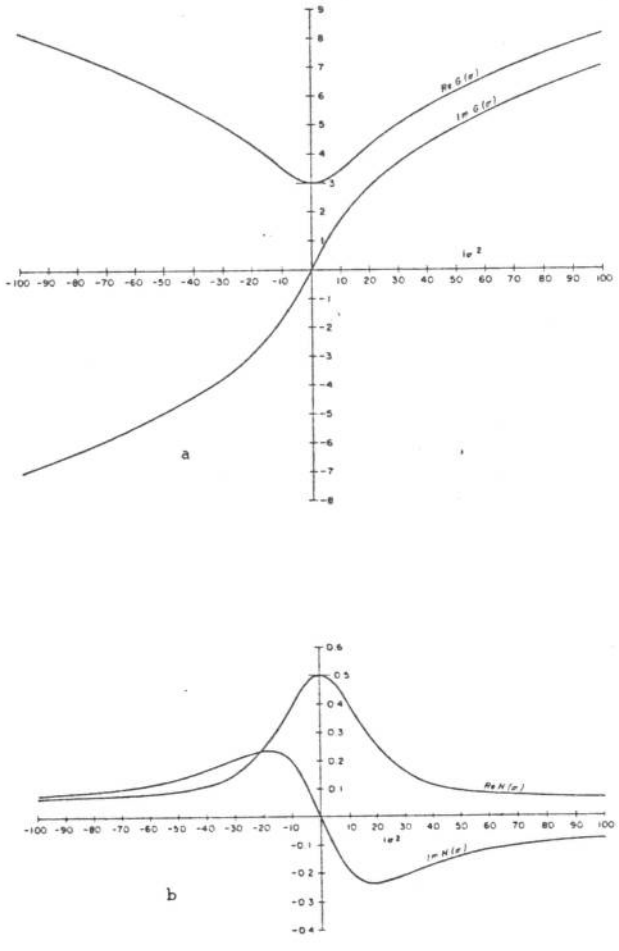

FIGURE 19.—(a) Plot of real and imaginary parts of $G(\sigma)$ against $i\sigma^2$. (b) Plot of real and imaginary parts of $H(\sigma)$ against $i\sigma^2$.

We first examine our experimental computations to determine for which values of β the actual operands approximate exponentials. (If $M=E^{i(\beta t+\phi)}$, then $\partial M/\partial t=i\beta M$, so $\beta=(1/iM)\partial M/\partial t$ where M is regarded as a complex valued function of time and space.) Empirically it was noticed that the transport field usually consists of a train of vortices along the storm's path; in general, these vortices do not travel or increase in strength with any great rapidity, suggesting that for the transport operand M, the value of β remains small, and a linear approximation may be acceptable.

The storm model used in this study is a previously determined analytic function, and moves with a uniform rectilinear motion. For this case, the time derivative of the forcing function can be written in the form

$$\frac{\partial}{\partial t}=-\mathbf{V}_s\cdot\nabla \tag{12}$$

where $\mathbf{V}_s$ is the storm velocity. The appearance of $\mathbf{V}_s$ suggests that the value of β might be too large to admit a linear approximation for $H(\sigma)$, acting on the storm stress operand R. This may be why the linear approximation of H acting on R in (7) gave spurious waves for fast moving storms.

It appears from empirical computations that dropping the J function in (9) [i.e., $H(\sigma)\simeq H_0(\sigma_0)$] gave results in our numerical computations that could be acceptable for the present state of art in storm surge computations. We wish to show that this holds for the fast moving storms through comparisons of computations using an exact rather than a linear approximation of $H(\sigma)$. One can determine an exact $H(\sigma)$ from the *storm model itself* by first forming at any local point:

$$R=R_0e^{i(t-t_0)(\alpha-i\beta)} \tag{13}$$

then using (12); for uniform rectilinear storm motion, we have,

$$\frac{\partial}{\partial t}=\alpha+i\beta=-\frac{1}{R}(\mathbf{V}_s\cdot\nabla)R. \tag{14}$$

Thus we can then form

$$\sigma^2=\frac{D^2}{\nu}[i(f+\beta)+\alpha]. \tag{15}$$

$H(\sigma)$, as shown in (11), has poles (zero denominator) and cannot be used directly in (7); there was no problem with poles when only the linear terms derived from the expansion of $H(\sigma)$ given by (8) were retained. Instead, we first reform (9) and approximate the last term as

$$C+\frac{J}{if}\frac{\partial}{\partial t}=\frac{1+H(\sigma)}{1+\dfrac{G(\sigma)-G_1(\sigma_0)}{D^2/\nu[\sigma^2-\sigma_0^2]}}. \tag{16}$$

If H and G are truncated as in (8) we recapture the left

side. The right side is now free of poles; its value is determined at each grid point when using (15). Several tests were made with (9) where in one case the J function was omitted and in another case the right side of (16) was used; except in a minor sense, there were no significant differences in the coastal surge profile with these two cases.

APPENDIX II

For numerical computations using finite difference forms, the following notation (Shuman [19]) will be employed:

$$\overline{U}_t^t=\frac{1}{2\Delta t}[U_{j,k}^{m+1}-U_{j,k}^{m-1}];\ \overline{U}^{xyy}=\frac{1}{16}\begin{vmatrix}1&2&1\\2&4&2\\1&2&1\end{vmatrix}U_{j,k}^m; \tag{17}$$

$$\overline{U}_x^{xyy}=\frac{1}{8\Delta s}\begin{vmatrix}-1&0&1\\-2&0&2\\-1&0&1\end{vmatrix}U_{j,k}^m;\ \overline{U}_y^{xxy}=\frac{1}{8\Delta s}\begin{vmatrix}1&2&1\\0&0&0\\-1&-2&-1\end{vmatrix}U_{j,k}^m.$$

The following finite difference form was applied to (10):

$$\overline{U}_t^t=f(A_t)_{j,k}U_{j,k}^{m-1}-gD_{j,k}[(B_r)_{j,k}\overline{h}_x^{xyy}-(B_t)_{j,k}\overline{h}_y^{xxy}]$$
$$+f(A_r)_{j,k}\overline{V}^{xyy}+\overline{\left[C_r^{(y)}\tau-C_t^{(z)}\tau-\frac{D}{\rho_a}\left(B_r\frac{\partial p}{\partial x}-B_t\frac{\partial p}{\partial y}\right)\right]}^{xxyy}$$
$$\overline{V}_t^t=f(A_t)_{j,k}V_{j,k}^{m-1}-gD_{j,k}[(B_r)_{j,k}\overline{h}_y^{xxy}+(B_t)_{j,k}\overline{h}_x^{xyy}] \tag{18}$$
$$+f(A_r)_{j,k}\overline{U}^{xyy}+\overline{\left[C_r^{(y)}\tau+C_t^{(x)}\tau-\frac{D}{\rho_a}\left(B_r\frac{\partial p}{\partial y}-B_t\frac{\partial p}{\partial x}\right)\right]}^{xyy}$$

where p is atmospheric pressure and the surface pressure gradients are derived from the model storm. There is little difference in the numerical results whether the A, B, C functions are placed inside or outside the operators given in (17); (18) is mixed in this respect.

The closed boundary at the shore was treated by a numerical scheme given by Harris and Jelesnianski [4] and Jelesnianski [5], when using (18):

$$h_{0,j}^m=\Bigg[4D_{1,k}h_{1,k}^m-D_{2,k}h_{2,k}^m-\frac{2\Delta s}{g(B_r)_{0,k}}\Bigg\{f(A_r)_{0,k}V^{m}{}_{0,k}{}^{(x)m}\tau_{0,k}$$
$$-(C_t)_{0,k}^{(y)}\tau_{0,k}^m+(B_r)_{0,k}\frac{1}{\rho_a}\left(\frac{\partial p}{\partial x}\right)_{0,k}^m-(B_t)_{0,k}\frac{1}{\rho_a}\left(\frac{\partial p}{\partial z}\right)_{0,k}^m \tag{19}$$
$$+g(B_t)_{0,k}D_{0,k}\left(\frac{\partial h}{\partial y}\right)_{0,k}^m\Bigg\}\Bigg]/[4D_{1,k}-D_{2,k}].$$

The term $(\partial h/\partial y)_{0,k}^m$ cannot be directly applied since h^m is not known on the boundary; tests made showed no significant differences in the coastal surge if the term was ignored, computed with time value $m-1$, or if an iterative process was used.

These forms are an adaptation of a finite difference scheme given by Shuman [19]. Note that the time increment of the dissipating terms were formulated at time $(m-1)$ rather than time (m). This procedure was necessary to prevent instability in the finite difference computations (Richtmyer [18]).

The continuity equation (1) becomes

$$\overline{h}_t^t=-\overline{U}_x^{xyy}-\overline{V}_y^{xxy}.$$

APPENDIX III

Observed surge data during storm conditions are of poor quality, awkwardly distributed, and too limited in quantity to effect a satisfactory comparison between

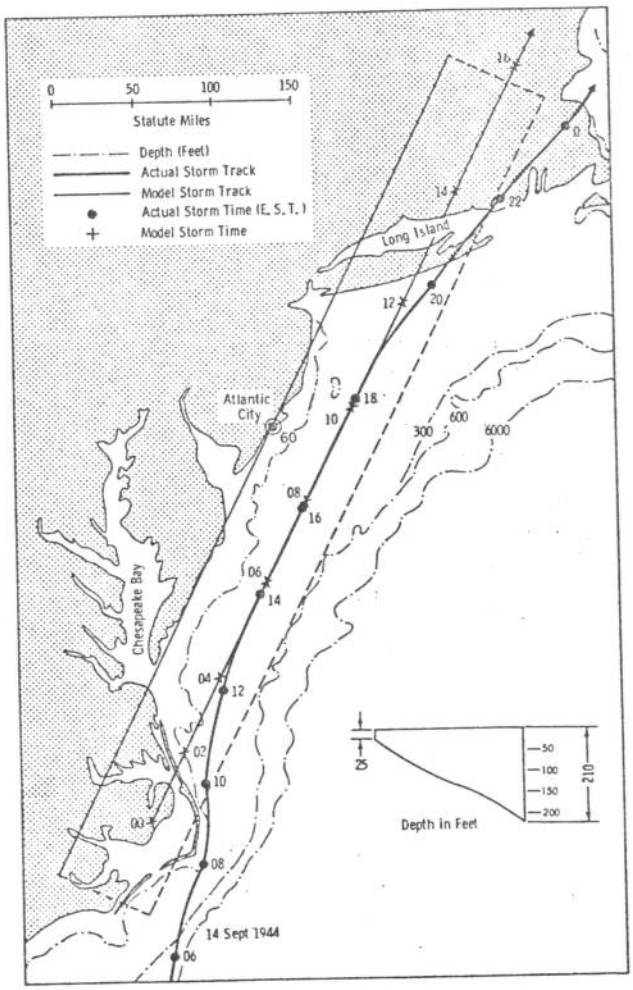

FIGURE 20.—Orienting a model basin along a portion of the Eastern Seaboard of the United States; the depths chosen for the one-dimensional model basin is shown in the insert, and is the mean depths about Atlantic City. The model track, simulating the natural storm track, for the September 1944 hurricane, is shown.

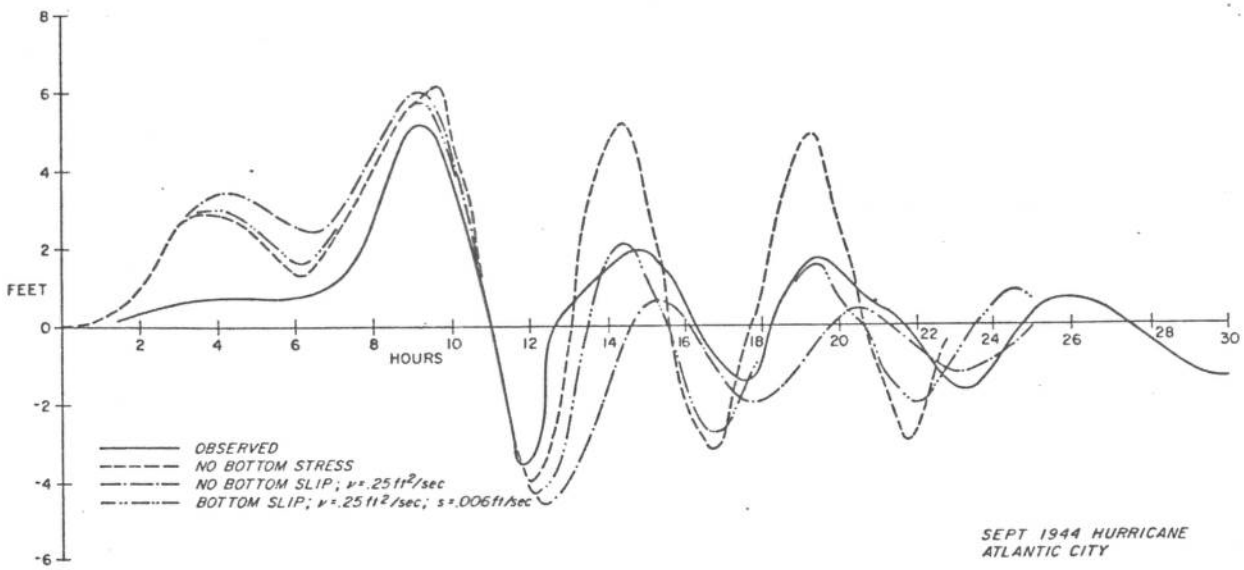

FIGURE 21.—Observed and computed surges, against time, at Atlantic City for the September 1944 storm. The basin used in the computations is given in figure 20. Hours are for model time.

observed and computed coastal surge profiles. This prevents a direct empirical approach to determine values for eddy and slip coefficients. However, the special phenomenon of observed *resurgences* at selected tide gages, generated by storms traveling parallel to the coast, can be used to determine plausible values for these coefficients, at least for fast moving storms.

Since actually observed trains of resurgences are irregular, we cannot readily obtain these coefficients by comparison of computed and observed amplitudes of resurgences in sequence. Instead, we shall compare the directly generated crest and following resurgences observed at Atlantic City against computed values; by appropriate variations of the slip and eddy coefficients, the amplitudes can be made to agree. Comparison of the remainder of the surge, observed and computed, against time will show whether additional modifications are necessary.

To demonstrate this method consider the path of a hurricane shown in figure 20. In this figure a rectangular, one-dimensional depth basin is oriented along the coast; the depth profile of the basin was derived from a mean approximation of the seaward depth off Atlantic City. The observed storm varied in strength, size, and speed with time (see [1]); it had a pressure drop of about 95 mb. off Cape Hatteras that decreased to about 30 mb. off Rhode Island; its radius of maximum winds decreased from 50 to 30 mi.; its speed increased from 25 to 35 m.p.h. These model parameters give a stationary storm maximum

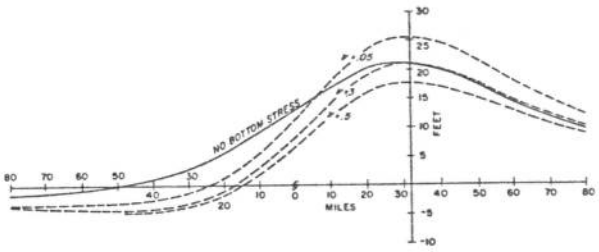

FIGURE 22.—Comparison of computed surge profiles, without and with bottom stress (equation (10)), generated by a fast moving storm traveling normal to the coast. The eddy viscosity coefficient ν ranges through an order of magnitude; no bottom slip.

wind of about 105 m.p.h. initially and decreasing to 65 m.p.h. off Rhode Island (fig. 2*). In computations described below, the model storm parameters, excepting latitude and storm direction, were changed at each hour of natural time as the storm moved across the basin; after passing Rhode Island, the model storm parameters remained constant.

This model storm and basin gave a computed surge, with resurgences, at Atlantic City as shown in figure 21 for various bottom stress conditions. The observed directly generated crest was translated to the time origin of

*The latitude of Atlantic City is used in the computations, consequently the winds are slightly different than given in figure 1.

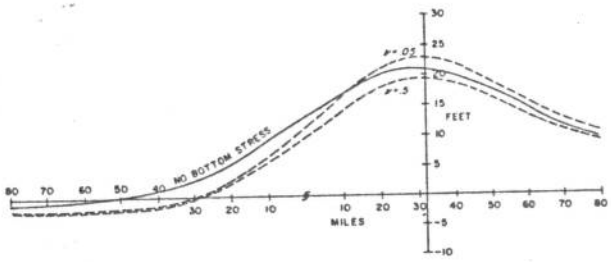

FIGURE 23.—Same as figure 22 with bottom slip s equal to 0.006 ft./sec.

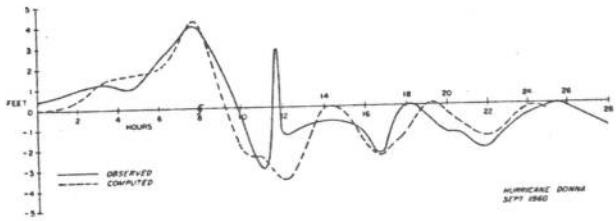

FIGURE 24.—Same as figure 21, for hurricane Donna. Eddy and slip coefficients were used in the computations.

the computed crests, i.e., model time. Notice that the computed surge without bottom stress has a directly generated crest that agrees with the observed crest but the computed resurgences are too large in amplitude; this suggests the need of a dissipating mechanism. The computed crests at time 4 hr. are the result of initialization phenomena due to rapid storm growth to maturity; a slower growth would suppress this precursor.

We wish to determine a value for an eddy viscosity coefficient that suppresses the resurgences computed without bottom stress but at the same time does not affect the directly generated crest. To do this we first digress to consider the effect of different eddy coefficient values on the directly generated surge. We consider at this time the case of a *zero* slip coefficient (no bottom stress) and plot the computed surge profile generated by a fast moving (30 m.p.h.) standard storm traveling normal to the coast in a standard basin (fig. 22). We consider further the case of an *infinite* bottom slip coefficient (no bottom current) and bracket the no bottom stress profile in the figure with profiles computed with eddy coefficients that range through an order of magnitude. The peak surge decreases monotonically with increasing eddy values for the range shown in the figure. Notice that small values of the eddy coefficient give a directly generated crest *larger* than computations without bottom stress. We now arbitrarily choose a middle value for the eddy coefficient of $\nu=0.25$ ft.^{2}/sec. and recompute the surge off Atlantic City.

For $\nu=.25$ ft.^{2}/sec., figure 21 shows that the directly generated crest is not significantly affected but the resurgences are dampened too strongly; there are also some changes in the period of the resurgences. Since the two flow conditions, frictionless flow and vanishing bottom current, did not adequately portray the resurgences, it was decided to use a bottom slip condition to better fit the computed and observed resurgences.

To determine the effects of bottom slip, we return to figure 22 and note that the profiles can be thought of as extremes; we then have a certain freedom in choosing the bottom slip coefficient between zero and infinity. Figure 23 illustrates how the profiles computed with stress in figure 22 were changed when incorporating a bottom slip coefficient of $s=0.006$ ft./sec. The smaller the slip value the closer the profiles approach the no-bottom-stress profile.

Figure 21 shows that when the above values for the eddy viscosity and slip coefficients are used the directly generated surge is not significantly affected by the bottom slip and the agreement between computed and observed resurgence amplitude is improved.

For an independent check of these coefficients, it was decided to repeat the computations for another storm, hurricane Donna, September 1960. Donna passed Atlantic City with its center about 35 mi. seaward. From data supplied by the Hydrometeorological Branch of the Weather Bureau, ESSA, the storm parameters used in the computations were: stationary-storm-maximum-wind 75 m.p.h. increasing by 0.5 m.p.h. each hour, radius of maximum wind constant at 40 mi., speed initially at 30 m.p.h. and accelerating at 0.667 mi./hr.^{2}; after passing Rhode Island, the storm parameters remained constant. Figure 24 illustrates the computed versus observed surge with time at Atlantic City. The observed secondary peak or spike at time 11½ hr. after initialization was not computed by the model. No explanation is given for this observed spike, whether it be dynamically or locally generated; it appears to be one of several higher harmonics, all of small amplitude, excepting the portrayed spike. It should be mentioned that the observed surges are best fit-by-eye curves from hourly observations supplied by the Coast and Geodetic Survey, ESSA; the observations were corrected for astronomical tide with the methods given by Harris [3]. The computed resurgences of both storms in this section are predominantly shelf seiches, but there were indications of edge or traveling waves but only of small amplitude.

Although the slip and eddy viscosity coefficient values were derived on the basis of fast moving storms passing over a basin equivalent to the seaward depths off Atlantic City, we use these same values when computing for slowly moving storms, and for all the basins encountered on the coastal shelf of the United States. We have done this for two reasons: in the first place, storms traveling at more than 10 m.p.h. give computed peak surges which have only minor differences whether bottom stress

used or not, and in the second place there are only few observations of storms traveling less than 10 m.p.h. (Harris [3]), and such observations as are available compare as well with the computed surges of this study as those of fast moving storms.

ACKNOWLEDGMENT

I am indebted to Dr. A. D. Taylor for his unstinting help and assistance in the preparation of this report. In particular I am grateful for his suggestions in the preparation of Appendix I where he introduced many of the mathematical concepts.

REFERENCES

1. H. E. Graham and G. N. Hudson, "Surface Winds Near the Center of Hurricanes (and Other Cyclones)," *National Hurricane Research Project Report* No. 39, U.S. Weather Bureau, Washington, D.C., Sept. 1960, 200 pp.
2. H. P. Greenspan, "The Generation of Edge Waves by Moving Pressure Distributions," *Journal of Fluid Mechanics*, vol. 1, No. 6, Dec. 1956, pp. 574–592.
3. D. L. Harris, "Characteristics of the Hurricane Storm Surge," *Technical Paper* No. 48, U.S. Weather Bureau, Washington, D.C., 1963, 139 pp.
4. D. L. Harris and C. P. Jelesnianski, "Some Problems Involved in the Numerical Solutions of Tidal Hydraulics Equations," *Monthly Weather Review*, vol. 92, No. 9, Sept. 1964, pp. 409–422.
5. C. P. Jelesnianski, "A Numerical Computation of Storm Tides by a Tropical Storm Impinging on a Continental Shelf," *Monthly Weather Review*, vol. 93, No. 6, June 1965, pp. 343–358.
6. C. P. Jelesnianski, "Numerical Computations of Storm Surges Without Bottom Stress," *Monthly Weather Review*, vol. 94, No. 6, June 1966, pp. 379–394.
7. K. Kajiura, "A Theoretical and Empirical Study of Storm Induced Water Level Anomalies," *Project* 202, Reference 59-23F, Texas A. & M. University, Department of Oceanography and Meteorology, Dec. 1956, 97 pp.
8. W. Munk, F. Snodgress, and G. Carrier, "Edge Waves on a Continental Shelf," *Science*, vol. 123, No. 3187, Jan. 1956, pp. 127–132.
9. T. Nomitsu, "A Theory of the Rising Stage of Drift Current in the Ocean: I. The Case of No Bottom Current," *Memoirs*, College of Science, Kyoto Imperial University (Series A), vol. 16, 1933, pp. 161–175.
10. T. Nomitsu, "A Theory of the Rising Stage of Drift Current in the Ocean: III. The Case of a Finite Bottom-Friction Depending on the Slip Velocity," *Memoirs*, College of Science, Kyoto Imperial University (Series A), vol. 16, 1933, pp. 309–331.
11. T. Nomitsu, "On the Development of the Slope Current and the Barometric Current in the Ocean: I. The Case of No Bottom-Current," *Memoirs*, College of Science, Kyoto Imperial University (Series A), vol. 16, 1933, pp. 203–241.
12. T. Nomitsu, "Coast Effect Upon the Ocean Current and the Sea Level: II. Changing State," *Memoirs*, College of Science, Kyoto Imperial University (Series A), vol. 16, 1934, pp. 249–280.
13. T. Nomitsu and T. Takegami, "On the Development of the Slope Current and the Barometric Current in the Ocean: II. Different Bottom Conditions Assumed," *Memoirs*, College of Science, Kyoto Imperial University (Series A), vol. 16, 1933, pp. 333–351.
14. T. Nomitsu and T. Takegami, "Coast Effect Upon the Ocean Current and the Sea Level: I. Steady State," *Memoirs*, College of Science, Kyoto Imperial University (Series A), vol. 16, 1934, pp. 93–141.
15. G. W. Platzman, "The Dynamical Prediction of Wind Tides on Lake Erie," *Meteorological Monographs*, vol. 4, No. 26, Sept. 1963, 44 pp.
16. R. O. Reid, "Modification of the Quadratic Bottom-Stress Law for Turbulent Channel Flow in the Presence of Surface Wind Stress," *Technical Memorandum* 93, U.S. Army Corps of Engineers, Beach Erosion Board, 1957, 33 pp.
17. R. O. Reid, "Effect of Coriolis Force on Edge Waves (1) Investigation of Normal Modes," *Journal of Marine Research*, vol. 16, No. 2, 1958, pp. 109–144.
18. R. D. Richtmyer, *Difference Methods for Initial-Value Problems*, Interscience Publishers, New York, 1957, 238 pp. (see p. 94).
19. F. Shuman, "Numerical Experiments with the Primitive Equations." *The Proceedings of the International Symposium on Numerical Weather Predictions, Tokyo, Nov. 7–13, 1960*, Meteorological Society of Japan, Tokyo, Mar. 1962, pp. 85–108.
20. P. Welander, "Numerical Prediction of Storm Surges," *Advances in Geophysics*, vol. 8, Academic Press, New York, 1961, pp. 315–379.

[Received January 30, 1967; revised July 26, 1967]